Colloid Polym Sci (2004) 282: 544–554
DOI 10.1007/s00396-003-0958-2

ORIGINAL CONTRIBUTION

Yuezhen Bin
Reiko Adachi
Tong Xu
Masaru Matsuo

Small-angle Hv light scattering from deformed spherulites with orientational fluctuation of optical axes

Received: 28 March 2003
Accepted: 26 June 2003
Published online: 12 December 2003

Y. Bin · R. Adachi · T. Xu
M. Matsuo (✉)
Department of Textile and Apparel Science,
Faculty of Human Life and Environment,
Nara Women's University,
630-8263 Nara, Japan
E-mail: m-matsuo@cc.nara-wu.ac.jp

Abstract Mathematical evaluation was done for small-angle light scattering from disordered spherulites under Hv polarization conditions. The calculation was carried out for a two-dimensional deformed spherulite whose major optical axes are oriented at 0 or 45° with respect to the radial direction. The calculated results were compared with the scattering patterns observed for polypropylene (PP) spherulites, whose optical axes are oriented parallel to the radial direction, and poly(butylene terephthalate) (PBT) spherulites, whose optical axes are oriented at 45° with respect to the radial direction. The degree of disorder for PBT was much larger than that for PP. By selecting a parameter associated with the degree of disorder of the optical axes with respect to the radial direction, the patterns calculated as a function of draw ratios were in good agreement with the observed patterns, which changed from four leaves to streaks extended in the horizontal direction. Through a series of observed and calculated patterns, it turns out that an increase in the disorder under the deformation process occurs drastically even for perfect spherulites in an undeformed state.

Introduction

Stein et al. [1, 2, 3, 4] and Samules [5, 6] have studied light scattering mainly from polymer spherulites both theoretically and experimentally in terms of Rayleigh–Gans theory. Another development has been carried out by Meeten and Navard in terms of the application of Mie theory to isotropic spheres [7]. They applied their concept to experiments concerning isotropic spheres and good results were obtained [8]. Apart from their complicated concept of Mie scattering [7, 8], this paper deals with disordered spherulites in a deformed state in terms of Rayleigh–Gans theory. Stein et al. considered perfect spherulites, the orientation of scattering elements with respect to the radius being the same everywhere within the spherulite [1, 2, 3, 4], and the complicated modification of the effect of internal spherulites [9]. Much has been learned about the deformation mechanism by uniaxial stretching. As Stein and Chu pointed out [10], the perfect-spherulite model leads to good quantitative predictions of the features of low-angle light scattering patterns. But the theoretical patterns differ quantitatively from experiments in two important aspects [4, 11]: (i) the theoretical patterns show a more rapid intensity decrease with angle at large scattering angles than do the experimental measurements; and (ii) the theory predicts a greater azimuthal angle dependence of scattered intensity than is experimentally found.

Figure 1 shows Hv light scattering patterns from positive spherulites observed for isotactic polypropylene films, which were molten-cast, annealed at 160 °C, and stretched uniaxially up to a draw ratio of $\lambda = 5$ at 135 °C [12], which were reported by Kawai more than 30 years ago. The scattering patterns are the well-known "four-leaf clover pattern" in the undeformed

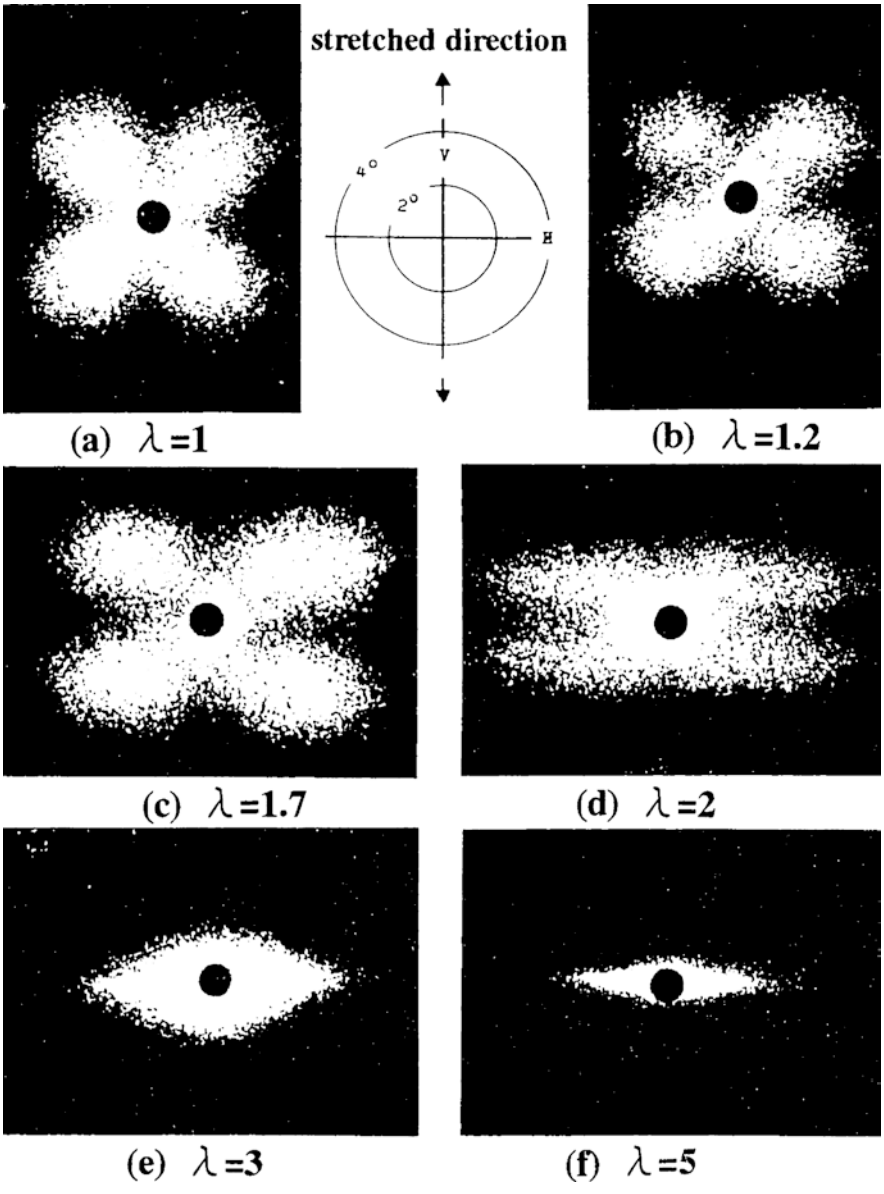

Fig. 1 Change of Hv light scattering patterns from isotactic polypropylene films stretched up to $\lambda = 5$. (These figures were reported in [12])

state and its modifications at drawn states up to $\lambda = 1.7$. In the undeformed state ($\lambda = 1$), the azimuthal angle dependence of the scattered intensity is less distinct than is experimentally found for polyethylene (G201) [13] and the theoretical pattern calculated from the perfect spherulite model [4]. The pattern changed from the four leaves to two streaks extended in the horizontal direction. This suggests a characteristic deformation of disordered spherulites predicting a disintegration of the normal spherulite. The theoretical scattering pattern from a perfect spherulite in the deformed state shows four scattering lobes extended in the horizontal direction. The patterns shown in Fig. 1 have sometimes been observed for crystalline polymer films with low crystallinity.

To solve these discrepancies, Stein and Chu carried out a theoretical treatment for light scattering from a two-dimensional undeformed spherulite having optical axes disordered with respect to the spherulite radius. They considered four special cases: (i) the disorder occurs in the radial direction only; (ii) the disorder occurs in the angular distribution only; (iii) there is combined radial and azimuthal disorder; and (iv) the optical axis makes a constant angle with the radius but there is disorder in the twist angle about the axis. In actual numerical calculations for cases (i) and (ii),

a correlation function for the disorder is defined as the ratio of the associated correlation distance to the radius of the spherulite. Since then a number of studies have been reported. Stein and Hashimoto have studied the effects of disorder of optical anisotropy with respect to the radius, in addition to the orientation disorder of optical axes on the scattering from an undeformed spherulite [11]. They also studied the effect of angular disorder of optical axes on the scattering from a deformed spherulite [14]. Furthermore, Yoon and Stein proposed a lattice theory of orientation disorder in a two-dimensional spherulite, in which the direction of orientation of the optical axis in lattice cells is allowed to deviate statistically from its mean value in a manner correlated with the orientation in neighboring cells [15]. Their results for two-dimensional spherulites show improved correspondence with observed scattering patterns. On the other hand, detailed analysis was done by considering the orientation disorder of lamellae with finite dimensions along the radial direction [16]. At that time, however, it was impossible to apply this complicated method to a deformed spherulite.

Anyway, there is no paper for the mathematical evaluation of the radial disorder of the optical axes within a deformed spherulite, in spite of a number of detailed analyses for undeformed spherulites discussed above. This is due to very complicated numerical calculations. Namely, the theoretical analysis of scattering patterns from disordered spherulites has never been reported as a function of draw ratios. Recent developments in the calculating speed and capacity of computers have provided the possibility to pursue numerical calculations from such a complicated system. The calculations have been concentrated on the deformation mechanism of perfect spherulites [17] and rods [18] in relation to the orientation distribution function of crystallites estimated by the X-ray diffraction technique. In these model systems, the orientation distribution of crystallites is dependent upon the radial distribution with respect to the stretching direction but is independent in the radial direction.

This paper reports the first trial to pursue the theoretical calculation of the disorder of orientation of the optical axes with respect to the radial direction. The calculation is carried out for a two-dimensional deformed spherulite. The results are compared with the scattering patterns observed for polypropylene (PP) and poly(butylene terephthalate)(PBT) [19, 20, 21, 22]. The former is known as a usual spherulite whose optical axes are oriented parallel to the radial direction, while the latter is an unusual spherulite whose optical axes are oriented at 45° with respect to the radial direction. The calculated patterns are analyzed in comparison with the scattering patterns observed for PP and PBT films.

Experimental methods and results

PBT pellets were obtained from Mitsubishi Chemical Co. Ltd. The pellets of PBT were pressed at 150 °C under 0.5 MPa and the molded specimen was immersed in ice water. The thickness of all the specimens was set to be less than 100 μm. This was done to obtain two-dimensional spherulites for analyzing Hv scattering from "unusual spherulites", which is very important to analyze the different deformation mechanisms between PP and PBT spherulites theoretically. The film was cut into strips of length 50 mm and width 20 mm. The strips were placed in a hot loven at 200 °C for 5 min and then elongated up to three times. After elongation, the specimens were maintained at elevated temperature for 20 min then cooled down to room temperature.

Small-angle light scattering (SALS) patterns under cross (Hv)-polarization conditions were obtained with a 15-mW He–Ne gas laser as a light source. Diffuse scattering was avoided by sandwiching the specimen between cover glasses with silicone oil as immersion fluid. The predominant orientation of benzene rings parallel to the film surface was confirmed by the X-ray diffraction pattern (end view) showing diffraction arcs.

Figure 2 shows the scattering patterns from PBT films prepared by compression molding and elongation at 200 °C. The observed variations in the scattering pattern indicate the different arrangement of the optical axes with respect to the radial direction. The pattern (a) in the undeformed state is a four-leaf clover type with scattering maximum at $\mu = 0$, 90, 180, and 270°, which is the scattering from so-called unusual spherulites. Such a pattern is characteristic of a spherulite whose optical axis lies at an angle close to $\pm 45°$ and has usually been found in the scattering from the spherulitic texture of PBT [16, 19, 20]. The pattern (a) in Fig. 1 indicates that the orientation of the major optical axes is fixed at 0° with respect to the radial direction. Namely, the two different patterns reflect difference in the principal polarizability of the crystal with respect to the spherulitic radius. It must, however, be restricted to the two-dimensional spherulite whose optical axes are oriented in the plane because, irrespective of the orientation of the optical axes with respect to the spherulitic radius, the scattered intensity exhibited a four-leaf clover type, like pattern (a), when the optical axes twist randomly or when the spherulite is of the three-dimensional type. The pattern from an undeformed PBT spherulite showing a clear μ dependence of the scattered intensity (see pattern (a) in Fig. 2) exhibits the type of scattering expected from perfect spherulites [1, 23], while pattern (a) in Fig. 1 indicates the scattering from disordered spherulites. As shown in Figs. 1 and 2, the scattering from spherulites at draw ratios lower than $\lambda = 2$ maintained the modification of the four-leaf clover pattern. But with further elongation, the pattern changed from the four leaves to two streaks extended in the horizontal direction.

Based on the observed patterns from PP and PBT spherulites, the theoretical calculation was carried out for Hv scattering from a two-dimensional spherulite as a function of draw ratio λ.

Theory

Figures 3a and b show radial disorder of the optical axes within undeformed and deformed spherulites. In the two models, the orientation of the optical axes is dependent upon the position along the radius.

According to Rayleigh–Gans theory [24], the amplitude of the light scattering may be given by

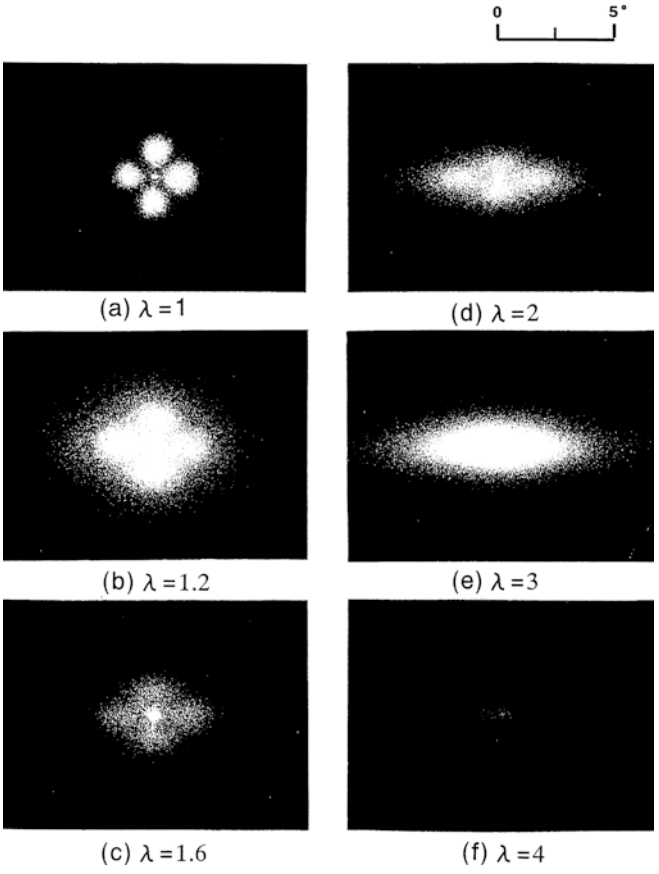

Fig. 2 Hv light scattering patterns from poly(butylene terephthalate) stretched up to $\lambda = 4$

$$E = C \int \rho_0 (\boldsymbol{M} \bullet \boldsymbol{O}) \exp\{ik(\boldsymbol{r} \bullet \boldsymbol{s})\}\, dr \tag{1}$$

where k is the wave number $2\pi/\lambda'$, with λ' the wavelength of light in the scattering medium. C is a constant and $\boldsymbol{s}$ is the scattering vector defined by $(\boldsymbol{s}_0 - \boldsymbol{s}')$, where $\boldsymbol{s}_0$ and $\boldsymbol{s}'$ are the vectors of incident and scattering beams, which is given by [1, 2, 3, 4, 5, 6]

$$\boldsymbol{s} = -\sin\theta \sin\mu\, \boldsymbol{j} - \sin\theta \cos\mu\, \boldsymbol{k} \tag{2}$$

where θ and μ are scattering and azimuthal angles, respectively. ρ_0 is the density of the scattering elements. M is the induced dipole moment of the scattering element located at a distance r from the center of the spherulite, and is given for vertical polarization of the polarizer by [1, 2, 3, 4, 5, 6]

$$\boldsymbol{M} = E_0[\delta(\boldsymbol{k} \bullet \boldsymbol{d})\boldsymbol{d} + b_t \boldsymbol{k}] \tag{3}$$

E_0 is the amplitude of the incident beam. The scattering element is assumed to have uniaxial anisotropy with polarizabilities $\alpha_{||}$ and $\alpha_{\perp}$ along and perpendicular to the optical axis, respectively. $\boldsymbol{d}$ is the unit vector along the optical axis in the undeformed state. If the polarizability in the surrounding medium of the spherulite is α_s, then $\delta = \alpha_{||} - \alpha_{\perp}$ and $b_t = \alpha_{||} - \alpha_s$. $(\boldsymbol{M} \bullet \boldsymbol{O})$ is an effective dipole moment of the scattering element located at r from the center of the spherulite under a given orientation of polarizer and analyzer. The unit vector $\boldsymbol{O}$ along the polarization direction of the analyzer for the horizontal polarization is given as $\boldsymbol{j}$ at very small scattering angle θ.

The scattered intensity is given by [1, 2, 3, 4, 5, 6]

$$I = C \int \rho_0 (\boldsymbol{M} \bullet \boldsymbol{O})_1 (\boldsymbol{M} \bullet \boldsymbol{O})_2 \exp\{-ik(\boldsymbol{r}_1 \bullet \boldsymbol{s})\} \exp\{-ik(\boldsymbol{r}_2 \bullet \boldsymbol{s})\} dr_1 dr_2 \tag{4}$$

If the orientation of the optical axis of the scattering element fluctuates around their average value ω_0, ω is a function of r like $\omega(r) = \omega_0 + \Delta(r)$, where $\Delta(r)$ is the local fluctuation of ω. In this viewpoint, the angle ω_1 at r_1 and ω_2 at r_2 may be given by $\omega_1 = \omega_0 + \Delta_1$ and $\omega_2 = \omega_0 + \Delta_2$, respectively. When the difference between orientation fluctuation Δ_1 at r_1 and Δ_2 at r_2 is given by Δ_{12}, the quantity Δ_{12} is defined by $\Delta_{12} = \Delta_2 - \Delta_1 = \omega_2 - \omega_1$; the angles ω_1 and ω_2 characterizing the relative

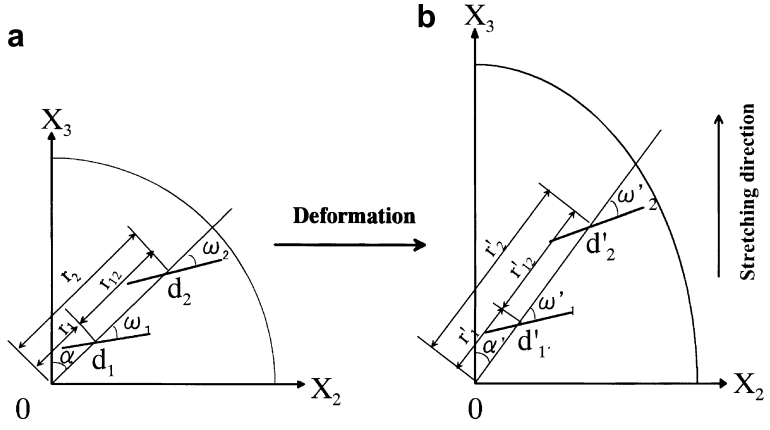

Fig. 3a,b Definition of the optical axes along the radial direction: **a** undeformed spherulite, **b** deformed spherulite

orientation of the optical axes of two scattering elements are separated by a distance $r_{12}=r_1-r_2$. In the present system, ω_0 is 0° for PP and 45° for PBT. The quantity Δ_{12} is related to the correlation function $f(r_{12})$, which is given by [10]

$$f(r_{12}) = \langle \cos 2\Delta_{12} \rangle_{r_{12}} \tag{5}$$

The correlation function which, in general, decreases asymptotically from unity to zero with increasing distance $|r_{12}|$ from zero, is assumed to be given by the empirical function [10]

$$f(r_{12}) = \exp\left\{\frac{-|r_{12}|}{a}\right\} \tag{6}$$

where a is the correlation distance. The empirical function was first introduced to analyze the orientation fluctuation of optical axes within a spherulite by Stein and Chu [10]. Equation 6 reduces to zero as a approaches zero and to unity as a is large.

Based on the general description of the theory of Stein and Stidham [25], the following relation can be obtained:

$$\left\langle \cos^2 n\Delta_{12} \right\rangle_{r_{12}} = \frac{1}{2}\left\{1 + \exp\left(\frac{-n^2|r_{12}|}{a}\right)\right\} \tag{7}$$

As discussed by Stein and Chu [10], the term $\cos 2\Delta_1$ varies randomly with r_1, so if one averages over all spherulites of the system, it will suffice to replace it with its average value $<\cos 2n\Delta_1>_{\mathrm{av}}$. Accordingly, we have

$$\left\langle \cos^2 n\Delta_1 \right\rangle_{\mathrm{av}} = \frac{1}{2} - \frac{1}{\left(n^2R/a\right)^2}\left\{1 - \frac{n^2R}{a} - \exp\left(\frac{-n^2R}{a}\right)\right\} \tag{8}$$

Thus we have

$$\left\langle \cos^2 2n\Delta_1 \right\rangle_{\mathrm{av}} = -\frac{2}{\left(n^2R/a\right)^2}\left\{1 - \frac{n^2R}{a} - \exp\left(\frac{-n^2R}{a}\right)\right\} \tag{9}$$

Obviously, Eq. 9 reduces to zero as a approaches zero indicating random behavior of the local fluctuation of ω, and to unity as a is large indicating no local fluctuation.

When the film is stretched along the X_3 axis, the spherulite may be deformed and the optical axes of the scattering elements within the spherulite may be oriented toward the stretching direction, so that Eq. 4 can be written as follows:

$$I = C\int \rho'(\boldsymbol{M}'\bullet\boldsymbol{O})_1(\boldsymbol{M}'\bullet\boldsymbol{O})_2 \exp\{-ik(\boldsymbol{r}'_1\bullet\boldsymbol{s})\} \times \exp\{-ik(\boldsymbol{r}'_2\bullet\boldsymbol{s})\}d\boldsymbol{r}'_1 d\boldsymbol{r}'_2 \tag{10}$$

where the primed notations correspond to the deformed state of the spherulite. The scattered intensity is then calculated for a certain model. The model in this paper is based on the assumption that (i) the spherulite is deformed toward the stretching direction according to the affine deformation process, and that (ii) the optical axes of the scattering elements within the spherulite are also oriented toward the stretching direction according to the affine deformation. As shown in Fig. 3, the position r at a given angle α is deformed into r' and oriented at angle α'. Accompanied by the deformation process, the optical axes of the scattering elements change their orientation from $(\alpha+\omega)$ to $(\alpha'+\omega')$ with respect to the stretching direction. Such deformation may be realized when the lamellae are composed of the scattering elements interconnected by a weak physical force.

The affine deformation of the spherulite leads to

$$\begin{aligned}\boldsymbol{r}' &= r'\{\sin\alpha'\boldsymbol{j} + \cos\alpha'\boldsymbol{k}\}\\ &= r\{\lambda_2\sin\alpha\boldsymbol{j} + \lambda_3\cos\alpha\boldsymbol{k}\}\end{aligned} \tag{11}$$

where λ_3 and λ_2 are elongation ratios imposed on the spherulite parallel and perpendicular to the stretching direction. The density of scattering elements within a spherulite is given by

$$\rho_0 dr = \rho' dr' \tag{12}$$

The optical axis in the deformed state is given by

$$\begin{aligned}\boldsymbol{d}' &= \sin(\alpha'+\omega')\boldsymbol{j} + \cos(\alpha'+\omega')\boldsymbol{k}\\ &= \frac{\lambda_2\sin(\alpha+\omega)\boldsymbol{j}+\lambda_3\cos(\alpha+\omega)\boldsymbol{k}}{\left[\lambda_2^2\sin^2(\alpha+\omega)+\lambda_3^2\cos^2(\alpha+\omega)\right]^{1/2}}\end{aligned} \tag{13}$$

Under Hv polarization conditions, $(\boldsymbol{M}\bullet\boldsymbol{O})_1(\boldsymbol{M}\bullet\boldsymbol{O})_2$ is given by

$$\begin{aligned}&(\boldsymbol{M}\bullet\boldsymbol{O})_1(\boldsymbol{M}\bullet\boldsymbol{O})_2\\ &= \frac{\lambda_2\sin(\alpha_1+\omega_1)\lambda_3\cos(\alpha_1+\omega_1)}{\lambda_2^2\sin^2(\alpha_1+\omega_1)+\lambda_3^2\cos^2(\alpha_1+\omega_1)}\\ &\quad\times\frac{\lambda_2\sin(\alpha_2+\omega_2)\lambda_3\cos(\alpha_2+\omega_2)}{\lambda_2^2\sin^2(\alpha_2+\omega_2)+\lambda_3^2\cos^2(\alpha_2+\omega_2)}\end{aligned} \tag{14}$$

In an undeformed state, we have $\lambda_3=\lambda_2=1$. Accordingly, Eq. 14 reduces to

$$\begin{aligned}(\boldsymbol{M}\bullet\boldsymbol{O})_1(\boldsymbol{M}\bullet\boldsymbol{O})_2 &= \sin(\alpha_1+\omega_1)\cos(\alpha_1+\omega_1)\\ &\quad\times\sin(\alpha_2+\omega_2)\cos(\alpha_2+\omega_2)\end{aligned} \tag{15}$$

Because of no correlation between α_1 and α_2 in Eq. 15, the scattered intensity can be written by simply using the Bessel function [10]. However, in a deformed state, the equation of the scattered intensity contains exponential functions in a denominator and the equation becomes very complicated. As discussed before, recent developments in the calculating speed and capacity of computers

provides one with the possibility to pursue numerical calculations for such a complicated system.

Let us consider such a complicated mathematical treatment. Equation 10 can be written as follows:

$$
\begin{aligned}
&I(\alpha_1, \alpha_2) \\
&= \int_{r_1=0}^{R} \int_{r_2=0}^{R} (\boldsymbol{M} \bullet \boldsymbol{O})_1 \exp\{ik(\boldsymbol{r}_1 \bullet s)\} r_1 (\boldsymbol{M} \bullet \boldsymbol{O})_2 \\
&\quad \times \exp\{-ik(\boldsymbol{r}_2 \bullet s)\} r_2 dr_2 dr_1 \\
&= \int_{r_1=0}^{R} \int_{r_{12}=-r_1}^{R-r_1} (\boldsymbol{M} \bullet \boldsymbol{O})_1 (\boldsymbol{M} \bullet \boldsymbol{O})_2 \exp\{ik(B-A) r_1\} \\
&\quad \times \exp\{ikBr_{12}\} r_1 (r_1 + r_{12}) dr_{12} dr_1 \qquad (16)
\end{aligned}
$$

where the coefficients in Eq. 16 as well as the further calculation procedure are described in the Appendix in detail.

Finally, the scattered intensity can be obtained by carrying out the integration of α_1 and α_2 independently as follows:

$$
I = \int_0^{2\pi} \int_0^{2\pi} I(\alpha_1, \alpha_2) d\alpha_1 d\alpha_2 \qquad (17)
$$

The numerical calculation is carried out by setting parameters, R/λ' and R/a. The series of expansions for Eq. 25 in the Appendix was done up to $m = 29$, which is the capacity limit of our computer used in this calculation.

Results and discussion

Figures 4 and 5 show the patterns calculated at $\omega_0 = 0$ and 45°, respectively, by the change in R/a. R/λ' is fixed to be 10. Incidentally, the orientation fluctuation of optical axes with respect to the radial direction becomes zero indicating no local orientation at $R/a = 0$ ($a \to \infty$), while the optical axes tend to random behavior of local fluctuation at very large values of R/a ($a \to 0$). At lower scattering angles, the disorder leads to a disturbance of the four-leaf clover type pattern associated with the scattering from a perfect spherulite. The pattern becomes circular with increasing R/a. Even so, the scattering at $\theta = 0°$ shows no maximum, reflecting the characteristic scattering from a spherulite. Comparing pattern (a) in Fig. 1 with that in Fig. 4 and also comparing pattern (a) in Fig. 2 with that in Fig. 5, the pattern (b) calculated at $R/a = 0.1$ (see Fig. 4) is close to the observed pattern (a) in Fig. 1 and the pattern (a) calculated at $R/a = 0$ (see Fig. 5) is close to the observed pattern (a) in Fig. 2. This exhibits the scattering from PP spherulites, showing distinct lobes which is the type of scattering expected from disordered spherulites, while that from PBT spherulites is the type from perfect spherulites.

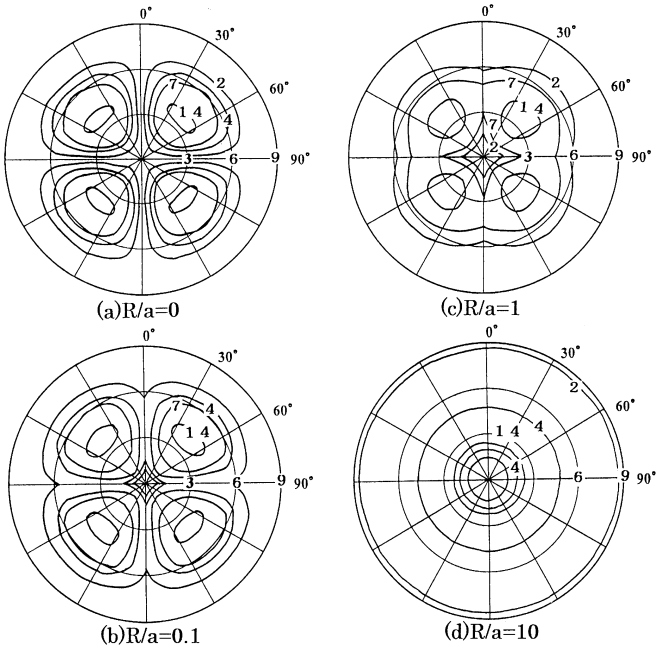

Fig. 4 Hv scattering patterns calculated at $\omega_0 = 0°$ as a function of R/a

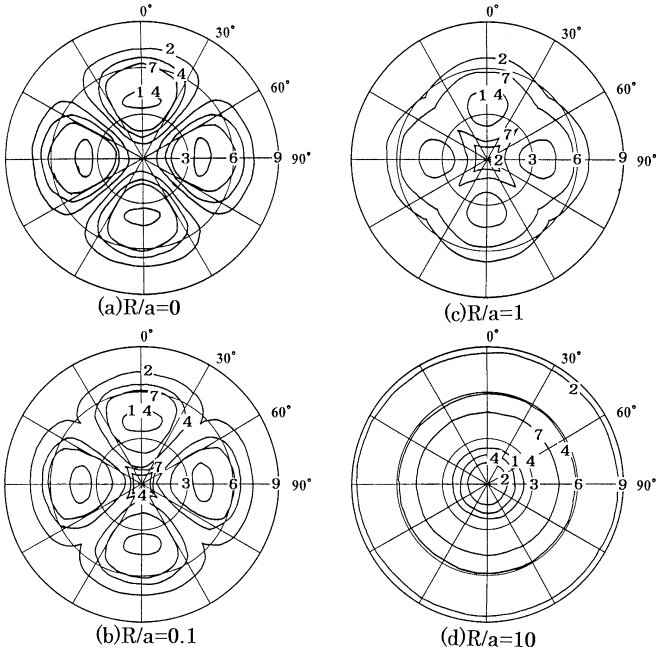

Fig. 5 Hv scattering patterns calculated at $\omega_0 = 45°$ as a function of R/a

Returning to Figs. 1 and 2, it is seen that the scattering lobes are extended in the horizontal direction with increasing draw ratio (λ). The patterns show a diffuse scattering in the azimuthal direction and the lowest intensity at a scattering angle of zero ($\theta = 0°$). This

tendency is observed for PBT indicating the existence of perfect spherulites in the undeformed state. Incidentally, we must emphasize that the cross-polarization condition in our instrument cannot remove the strong incident beam as shown in Figs. 1 and 2; then the strong spots at $\theta = 0°$ are a sort of artifact.

The patterns from PP and PBT spherulites at $\lambda \geq 3$ show similar profiles taking two streaks extended in the horizontal direction. These patterns predict a drastic increase in the disordering degree of orientation of the optical axes with respect to the radial direction, indicating a disintegration of spherulites by further elongation.

However, there is no report on the analysis of the above demonstration in terms of theoretical aspects. In this paper, the calculated patterns from deformed spherulites are presented as a function of R/a. Figures 6, 7, and 8 show the patterns calculated at $\omega_0 = 0°$ and Figs. 9, 10, and 11, at $\omega_0 = 45°$; Figs. 6 and 9 are calculated at $\lambda = 1.5$, Figs. 7 and 10 at $\lambda = 2$, and Figs. 8 and 11 at $\lambda = 3$. With increasing R/a, the scattering lobes become indistinct indicating that the orientation of optical axes becomes more pronounced. The patterns show two streaks extended in the horizontal direction, independent of the value of ω_0, when R/a is selected beyond unity. The change in pattern from four leaves to two streaks extended in the horizontal direction is due to an increase in the orientational disorder of the optical axes with respect to the radial direction. At the same value of R/a, the scattering lobes with increasing draw ratio are extended in the horizontal direction, maintaining an indistinct profile characterizing orientation fluctuation of the optical axes with respect to the radial direction.

By selecting a suitable value of R/a at each draw ratio, the calculated patterns are in good agreement with the observed ones. If there is no disorder for the orientation of the optical axes, the pattern shows clear scattering lobes extended in the horizontal direction, as reported by Clough et al. [4].

Judging from the comparison between the observed and the calculated patterns, the change in pattern with draw ratio indicates that the drastic increase in the orientational disorder of the optical axes appears even for perfect spherulites of PBT in an undeformed state. This is probably due to disintegration of perfect spherulites by complicated orientation of crystallites within a lamella, as well as the disruption of unstable crystal lamellae leading to strain in the tie molecules.

Finally, we expect that further theoretical analysis of polarized light scattering from more complicated systems may be possible and may provide a progressive advance in polymer solid and liquid crystal physics. Small-angle light scattering under polarization conditions provides information concerning the deformation mechanism of superstructures such as spherulites and rod-like textures, as well as the orientation of optical axes within the superstructures. To understand the detailed characteristics of crystalline polymers, the Hv light scattering technique is thought to be more useful by combining it with the experimental results obtained

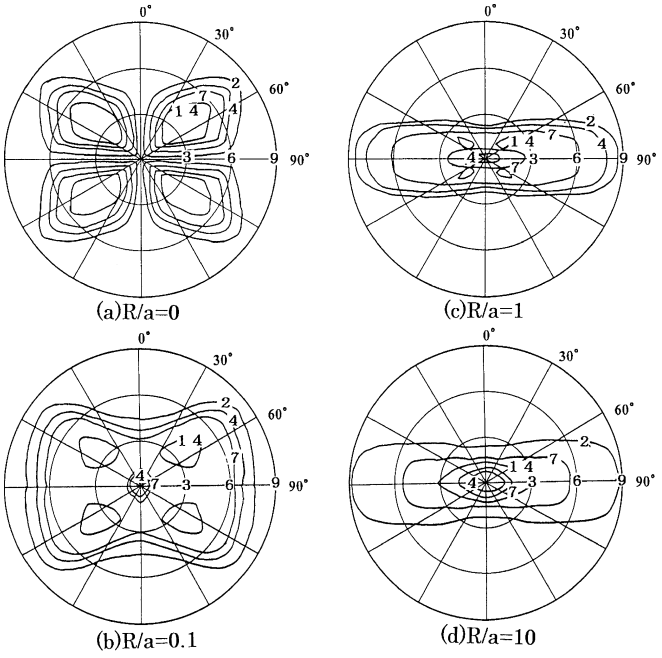

Fig. 6 Hv light scattering patterns calculated at $\omega_0 = 0°$ and $\lambda = 1.5$

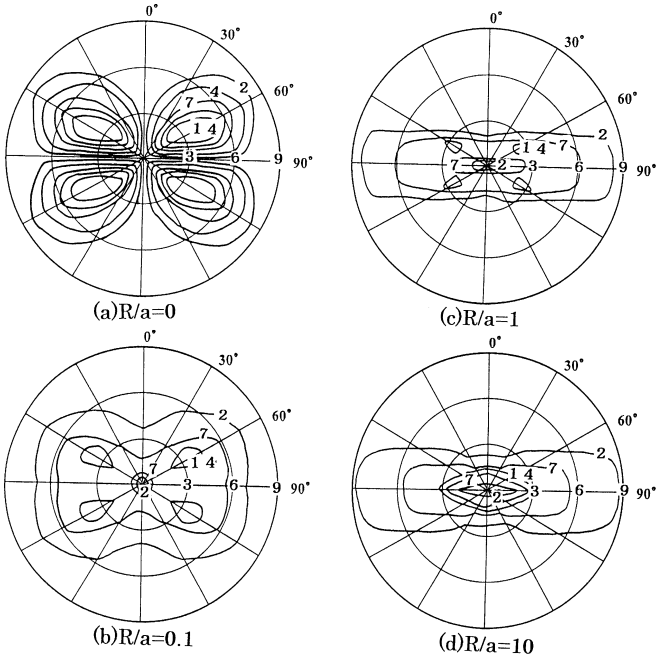

Fig. 7 Hv light scattering patterns calculated at $\omega_0 = 0°$ and $\lambda = 2$

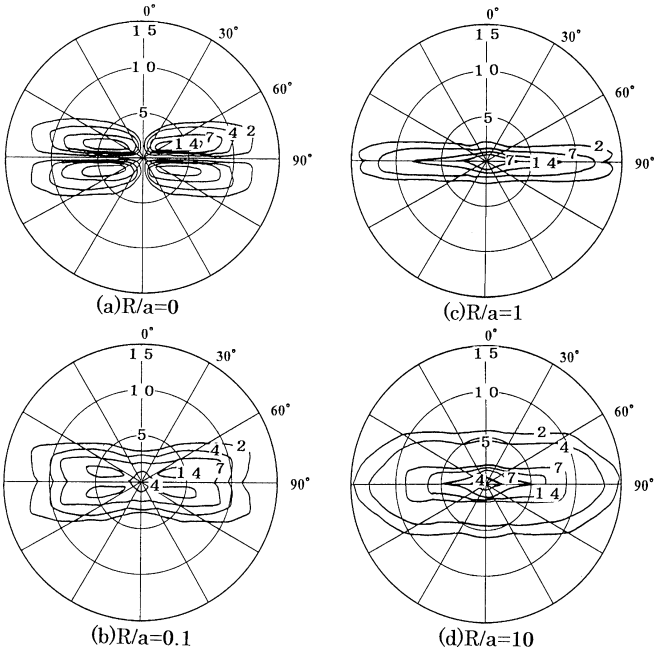

Fig. 8 Hv light scattering patterns calculated at $\omega_0 = 0°$ and $\lambda = 3$

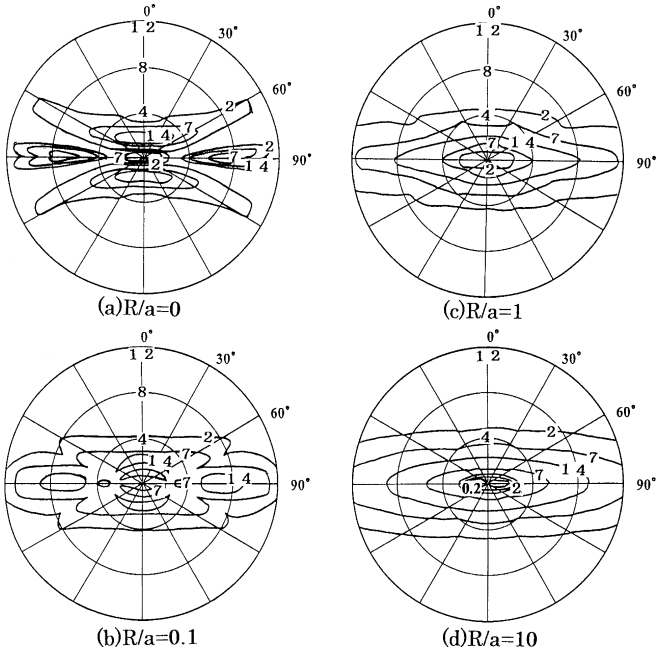

Fig. 10 Hv light scattering patterns calculated at $\omega_0 = 45°$ and $\lambda = 2$

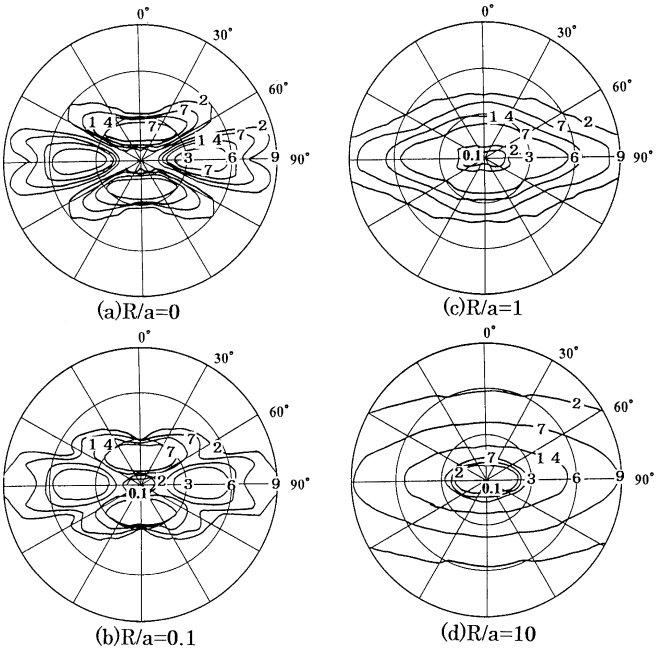

Fig. 9 Hv light scattering patterns calculated at $\omega_0 = 45°$ and $\lambda = 1.5$

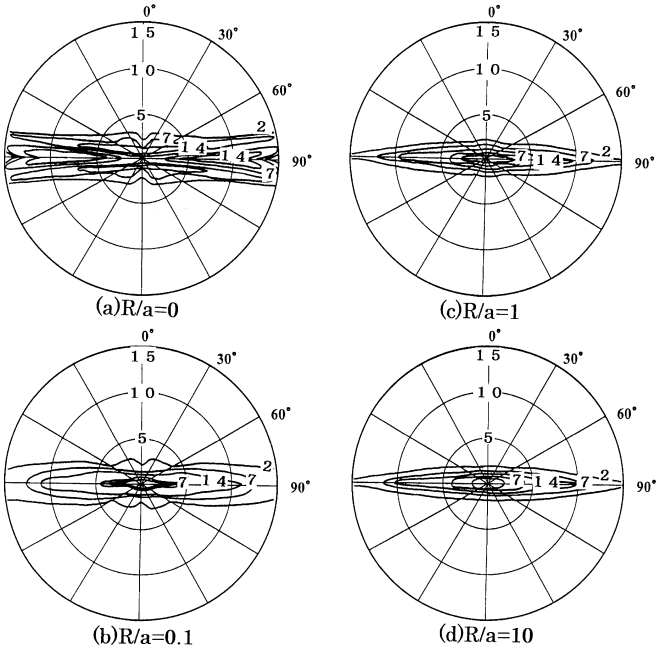

Fig. 11 Hv light scattering patterns calculated at $\omega_0 = 45°$ and $\lambda = 3$

by X-ray diffraction and birefringence. This method was adopted for polyethylene with high crystallinity, since the optical axes are thought to be equivalent to the crystal *c*-axes [17]. This analysis will be applied to other polymers with lower crystallinity than polyethylene, such as PBT, poly(ethylene terephthalate), and nylon 66. Actually, some important papers using PBT as an example have been published covering manufacturing aspects of processing [26, 27, 28] and polymer blends [29].

Conclusion

Mathematical evaluation of small-angle light scattering under Hv polarization conditions was done for a deformed spherulite with disorder of the orientation of the optical axes with respect to the radial direction. The calculation was carried out for a two-dimensional deformed spherulite whose major optical axes are oriented at 0 and 45° with respect to the radial direction. The calculated results were compared with the scattering patterns observed for polypropylene (PP) and poly(butylene terephthalate) (PBT) spherulites. The former is known to have usual spherulites whose optical axes are oriented parallel to the radial direction, while the latter has unusual spherulites whose optical axes are oriented at 45° with respect to the radial direction. By selecting a parameter associated with the degree of disorder of the optical axes with respect to the radial direction, the patterns calculated as a function of draw ratio were in good agreement with the observed patterns, which changed from four leaves to streaks extended in the horizontal direction. Through a series of observed and calculated patterns, it turned out that an increase in disorder occurs under the deformation process, indicating complicated orientation of the optical axes due to strain of tie molecules within the spherulite. This is probably due to the disruption of unstable crystal lamellae within the PP and PBT spherulites.

Appendix

The coefficients A and B in Eq. 16 are given by

$$A = \lambda_3 \cos\alpha_1 \sin\theta \cos\mu + \lambda_2 \sin\alpha_1 \sin\theta \sin\mu \tag{18}$$

$$B = \lambda_3 \cos\alpha_2 \sin\theta \cos\mu + \lambda_2 \sin\alpha_2 \sin\theta \sin\mu \tag{19}$$

Substituting $\omega_1 = \omega_0 + \Delta_1$, $\omega_2 = \omega_0 + \Delta_2$, and $\Delta_{12} = \Delta_2 - \Delta_1 = \omega_2 - \omega$, Eq. 14 reduces to

$$(\boldsymbol{M}\bullet\boldsymbol{O})_1(\boldsymbol{M}\bullet\boldsymbol{O})_2 = \frac{\lambda_2^2\lambda_3^2\{\cos 2(\alpha_1-\alpha_2) - \cos 2(\alpha_1+\alpha_2+2\omega_0)\cos 2\Delta_1\}f(r_{12})}{8\left\{\left(\lambda_2^4 + A'\lambda_2^2 + \frac{A'^2}{4}\right) + \left(\frac{A'}{2}\lambda_2^2 + \frac{A'^2}{4}\right)D + \frac{A'^2}{4}F\right\}} \tag{20}$$

where

$$A' = \lambda_3^2 - \lambda_2^2 \tag{21-1}$$

$$D = \cos\{2(\alpha_1+\omega_0)\}\cos 2\Delta_1 + \cos\{2(\alpha_2+\omega_0+\Delta_1)\}f(r_{12}) \tag{21-2}$$

$$F = \cos 2(\alpha_1+\omega_0)\cos 2\Delta_1 \cos 2(\alpha_2+\omega_0+\Delta_1)f(r_{12}) \tag{21-3}$$

By using Eq. 6, Eq. 20 can be rewritten as follows:

$$\begin{aligned}(\boldsymbol{M}\bullet\boldsymbol{O})_1(\boldsymbol{M}\bullet\boldsymbol{O})_2 &= \frac{C''\exp\left(-\frac{|r_{12}|}{a}\right)}{8\left\{A'' + B''\exp\left(-\frac{|r_{12}|}{a}\right)\right\}} \\ &= \frac{C''}{8}\left\{\frac{\exp\left(-\frac{|r_{12}|}{a}\right)}{A''} - \frac{B''\exp\left(-2\frac{|r_{12}|}{a}\right)}{A''^2}\right. \\ &\quad + \frac{B''^2\exp\left(-3\frac{|r_{12}|}{a}\right)}{A''^3} - \frac{B''^3\exp\left(-4\frac{|r_{12}|}{a}\right)}{A''^4} \\ &\quad \left. + \frac{B''^4\exp\left(-5\frac{|r_{12}|}{a}\right)}{A''^5} - \cdots\right\} \\ &= \frac{C''}{8}\sum_{m=1}^{\infty}(-1)^{m-1}\frac{(B'')^{m-1}\exp\left(-\frac{m|r_{12}|}{a}\right)}{(A'')^m}\end{aligned} \tag{22}$$

where

$$A'' = G + H\cos(2\alpha_1)\cos(2\omega_0) - H\sin(2\alpha_1)\sin(2\omega_0) \tag{23-1}$$

$$\begin{aligned}B'' = {} & \frac{J}{2}\cos(2\alpha_1)\cos(2\alpha_2)\cos^2(2\omega_0) \\ & + \frac{J}{2}\cos(2\alpha_1)\cos(2\alpha_2)\cos^2(2\omega_0)\cos(4\Delta_1) \\ & + \frac{J}{2}\sin(2\alpha_1)\sin(2\alpha_2)\cos^2(2\omega_0) \\ & - \frac{J}{2}\sin(2\alpha_1)\sin(2\alpha_2)\cos^2(2\omega_0)\cos(4\Delta_1) \\ & + H\cos(2\alpha_1)\cos(2\alpha_2)\cos(2\omega_0) \\ & - J\sin(2\alpha_1)\cos(2\alpha_2)\sin(2\omega_0)\cos(4\Delta_1) \\ & - J\cos(2\alpha_1)\cos(4\Delta_1)\sin(2\omega_0)\sin(2\alpha_2)\cos(2\omega_0) \\ & + \frac{J}{2}\cos(2\alpha_1)\cos(2\alpha_2)\sin^2(2\omega_0) \\ & - \frac{J}{2}\cos(2\alpha_1)\cos(4\Delta_1)\cos(2\alpha_2)\sin^2(2\omega_0) \\ & + \frac{J}{2}\cos(2\alpha_1)\sin^2(2\omega_0)\sin(2\alpha_2) \\ & + \frac{J}{2}\sin(2\alpha_1)\sin(2\alpha_2)\sin^2(2\omega_0)\cos(4\Delta_1) \\ & - H\cos(\Delta_1)\sin(2\omega_0)\sin(2\alpha_2)\end{aligned} \tag{23-2}$$

$$
\begin{aligned}
C'' = & -\cos(2\alpha_1)\cos(4\Delta_1)\cos(2\alpha_2)\cos^2(2\omega_0) \\
& +\cos(4\Delta_1)\sin(2\alpha_1)\sin(2\alpha_2)\cos^2(2\omega_0) \\
& +2\cos(4\Delta_1)\cos(2\alpha_2)\sin(2\alpha_1)\sin(2\omega_0)\cos(2\omega_0) \\
& +2\cos(2\alpha_1)\cos(4\Delta_1)\sin^2(2\omega_0)\sin(2\alpha_2) \\
& +\cos(2\alpha_1)\cos(2\alpha_2)-\cos(4\Delta_1)\sin(2\alpha_1)\sin^2(2\omega_0) \\
& +\sin(2\alpha_1)\sin(2\alpha_2)
\end{aligned}
\tag{23-3}
$$

where

$$
G=\lambda_2^4+\left(\lambda_3^2-\lambda_2^2\right)\lambda_2^2+\frac{\lambda_3^2-\lambda_2^2}{4} \tag{24-1}
$$

$$
H=\frac{\left(\lambda_3^2-\lambda_2^2\right)\lambda_2^2}{2}+\frac{\lambda_3^2-\lambda_2^2}{4} \tag{24-2}
$$

$$
J=\frac{\left(\lambda_3^2-\lambda_2^2\right)^2}{4} \tag{24-3}
$$

Substituting Eqs. 23-1, 23-2, 23-3 and 24-1, 24-2, 24-3 into Eq. 16, we have

$$
\begin{aligned}
I(\alpha_1,\alpha_2) = & \int_0^R \int_{-r_1}^{R-r_1} \frac{1}{16}\lambda_2^2\lambda_3^2 C'' \sum_{m=1}^{\infty}(-1)^{m-1}\frac{B''}{A'}\exp\left(m\frac{-|r_{12}|}{a}\right) \\
& \times[\cos k\{(A-B)r_1+Br_{12}\} \\
& +\cos k\{(A-B)r_1-Br_{12}\}] \\
& \times r_1(r_1+r_{12})dr_{12}dr_1 \\
= & \frac{\lambda_2^2\lambda_2^3(B'')^{m-1}C''(-1)^m-1}{16(A'')^m}\sum_{m=1}^{\infty}\{H_1(m)+H_2(m) \\
& -H_3(m)+H_4(m)-H_5(m)+H_6(m)\}
\end{aligned}
\tag{25}
$$

where

$$
H_1(m)=\frac{2\left\{\frac{a}{m}k^2R^2\sin\{k(A+B)R\}+2\frac{a}{m}kR(A+B)\cos\{(A+B)R\}-2a\ \sin\{k(A+B)R\}\right\}}{\{k(A+B)\}^3\left\{\left(\frac{a}{m}\right)^2(kB)^2+1\right\}} \tag{26-1}
$$

$$
H_2(m)=\frac{4\left\{\left(\frac{a}{m}\right)^3k^2(A+B)BR\cos\{k(A+B)R\}-a^3\ kB\sin\{k(A+B)R\}\right\}}{(kB)^2\left\{\left(\frac{a}{m}\right)^2(kB)^2+1\right\}^2} \tag{26-2}
$$

$$
H_3(m)=\frac{4\left\{\left(\frac{a}{m}\right)^3k^2B(A-B)R\cos\{k(A-B)R\}-\left(\frac{a}{m}\right)^3\ kB\sin\{k(A-B)R\}\right\}}{\left\{\left(\frac{a}{m}\right)^2(kB)^2+1\right\}^2\{k(A-B)\}^2} \tag{26-3}
$$

$$
\begin{aligned}
H_4(m)= & \frac{2\left(\frac{a}{m}\right)^2\left\{\left(\frac{a}{m}\right)^2B^2-1\right\}\left(\frac{a}{m}\right)e^{-mR/a}}{\left\{\left(\frac{a}{m}\right)^2B^2+1\right\}^2\left\{\left(\frac{a}{m}\right)^2A^2+1\right\}^2}\left[\cos AR\left\{A^2\left(\frac{a}{m}\right)^3-A^2R\left(\frac{a}{m}\right)^2-\left(\frac{a}{m}\right)-R\right\}\right. \\
& \left.+\left(\frac{a}{m}\right)A\sin AR\left\{\left(\frac{a}{m}\right)^2RA^2+2\left(\frac{a}{m}\right)+R\right\}\right]
\end{aligned}
\tag{26-4}
$$

$$
H_5(m)=\frac{\left(\frac{a}{m}\right)^2\left\{\left(\frac{a}{m}\right)^2A^2-1\right\}}{\left\{\left(\frac{a}{m}\right)^2A^2+1\right\}^2} \tag{26-5}
$$

$$
\begin{aligned}
H_6(m)= & \frac{1}{\left\{\left(\frac{a}{m}\right)^2A^2+1\right\}^2\left\{\left(\frac{a}{m}\right)^2B^2+1\right\}^2} \\
& \times\left[2\left(\frac{a}{m}\right)^2\left\{-A^2\left(\frac{a}{m}\right)^3e^{-mR/Ra}+A^2\left(\frac{a}{m}\right)^3\cos(AR)\right.\right. \\
& +A^3\left(\frac{a}{m}\right)^3R\sin(AR)+A^2\left(\frac{a}{m}\right)^2R\cos(AR) \\
& -2A\left(\frac{a}{m}\right)^2\sin(AR)-\left(\frac{a}{m}\right)\cos(AR) \\
& \left.+A\left(\frac{a}{m}\right)R\sin(AR)+\left(\frac{a}{m}\right)R-Rm/a+R\cos(AR)\right\} \\
& \times\left\{B^2\left(\frac{a}{m}\right)^3\cos(BR)+B^3R\left(\frac{a}{m}\right)^3\sin(BR)\right. \\
& -B^2\left(\frac{a}{m}\right)^2r\cos(BR)+2\left(\frac{a}{m}\right)B\sin(BR) \\
& \left.\left.-\left(\frac{a}{m}\right)\cos(BR)+BR\left(\frac{a}{m}\right)\sin(BR)-R\cos(BR)\right\}\right]
\end{aligned}
\tag{26-6}
$$

In numerical calculation, the intensity is normalized by R^4 and $H_1(m)$, for example, is rewritten as follows:

$$H_1(m) = \frac{2\left\{\frac{a}{mR}\left(\frac{2\pi R}{\lambda'}\right)^2 \sin\left\{\frac{2\pi R}{\lambda'}(A+B)\right\} + \frac{2a}{mR}\left(\frac{2\pi R}{\lambda'}\right)(A+B)\cos\left\{\frac{2\pi R}{\lambda'}(A+B)\right\} - \frac{2a}{R}\sin\left\{\frac{2\pi R}{\lambda'}(A+B)\right\}\right\}}{\left\{\frac{2\pi R}{\lambda'}(A+B)\right\}^3\left\{\left(\frac{a}{mR}\right)^2\left(\frac{2\pi R}{\lambda'}B\right)^2 + 1\right\}} \tag{27}$$

Similar treatment can also be applied to $H_2(m)$–$H_6(m)$.

References

1. Stein RS, Rhodes MB (1960) J Appl Phys 31:1873
2. Stein RS, Rhodes MB, Stidham SN (1962) Pure Appl Chem 4:219
3. Stein RS, Wilson PR, Stidham SN (1961) J Appl Phys 32:46
4. Clough RS, van Aartsen JJ, Stein RS (1965) J Appl Phys 36:3072
5. Samules RJ (1966) J Polym Sci C 13:37
6. Samules RJ (1974) J Polym Sci Polym Phys 12:1417
7. Meeten GH, Havard P (1989) J Polym Sci B 27:2023
8. Meeten GH, Havard P (1989) J Polym Sci B 27:2037
9. Prud'Homme RE, Yoon D, Stein RS (1973) J Polym Sci Polym Phys 11:1054
10. Stein RS, Chu W (1970) J Polym Sci A2 8:1137
11. Hashimoto T, Stein RS (1971) J Polym Sci A2 9:1747
12. Kawai H (1969) Proc 5th Int Congr Rheol 1:97–130
13. Motegi M, Oda T, Moritani M, Kawai H (1970) Polymer J 1:209
14. Stein RS, Hashimoto T (1971) J Polym Sci A2 9:517
15. Yoon DY, Stein RS (1974) J Polym Sci Polym Phys 12:763
16. Matsuo M, Geshi K, Moriyama A, Sawatari C (1982) Macromolecules 15:193
17. Matsuo M, Xu C (1997) Polymer 38:4311
18. Sugiura Y, Matsuo M (2001) Colloid Polym Sci 279:348
19. Seymour RW, Overton JR, Cooper SL (1975) Macromolecules 8:331
20. Schen M, Mehra U, Niinomi M, Koberstein JT, Cooper SL (1974) J Appl Phys 45:4182
21. Lilanoitku A, West JC, Cooper SL (1976) J Macromol Sci Phys B 12:563
22. Sawatari C, Muranaka T, Matsuo M (1983) Polymer J 15:33
23. Matsuo M, Ihara K (1982) J Polym Sci Polym Phys 20:1
24. van de Hulst HC (1957) Light scattering by small particles. Wiley, New York
25. Stein RS, Stidham SN (1964) J Appl Phys 35:42
26. Carr PL, Jakeways R, Klein JL, Ward IM (1997) J Polym Sci Polym Phys 35:2465
27. Ambroziak M, Gruin I, Wronikowski M, Zdunek K (2002) J Appl Polym Sci 86:2130
28. Racco T, Pegoretti A (2002) J Polym Sci Polym Phys 40:236
29. Liau WB, Liu AS, Chiu WY (2002) Macromol Chem Phys 203:294